Resolved resonance region evaluations of n+ ^{206,207,208}Pb for fast spectrum applications☆

Peter Brain [a,*], Yaron Danon [a], Dave Brown [b], Devin Barry [c], Amanda Lewis [c], Tim Trumbull [c], Toshihiko Kawano [d]

[a] *Rensselaer Polytechnic Institute, 3021 Tibbits Ave, Troy, 12180, NY, USA*
[b] *Brookhaven National Laboratory, 98 Rochester St, Upton, 11973, NY, USA*
[c] *Naval Nuclear Laboratory, 2401 River Road, Niskayuna, 12309, NY, USA*
[d] *Los Alamos National Laboratory, 87545, NM, USA*

ABSTRACT

Resolved resonance region evaluations of the major isotopes of natural lead, ^{206}Pb, ^{207}Pb, ^{208}Pb, have been performed to support the development of Generation IV reactors. Validation of nuclear data for lead fast reactors was performed with simulations of shielding benchmarks, integral critical benchmarks, and quasi-differential scattering measurements. Sensitivity analyses of these systems showed that elastic scattering reactions above 100 keV were the dominant reactions driving system performance. The resolved resonance regions (RRRs) of the lead isotopes extend past 100 keV, making the RRR an ideal starting point to evaluate lead cross sections. Since the R-matrix requires knowledge of bound, distant, and observed resonances, it was necessary to evaluate from 10^{-5} eV up to the respective limit of the RRR. The ^{208}Pb RRR evaluation was extended to 1.5 MeV in order to obtain resonance parameters used to calculate new elastic scattering angular distributions up to 1.5 MeV. Resonance parameter uncertainties and covariance were generated using the R-matrix code SAMMY. The new RRR parameters show a direct improvement to the scattering kernel below 1.5 MeV which in turn greatly improves fast critical experiments over ENDF/B-VIII.0.

1. Introduction

Molten lead and lead-bismuth eutectic are considered attractive candidates for coolants in generation-IV (GEN-IV) reactors due to superb neutron and thermal properties (Smith, 2010). Lead is one of two metals envisioned as coolants for liquid metal reactors, the other being sodium. While similar thermal properties can be achieved with either metal, lead maintains a negative void coefficient which is not the case for all sodium designs (dos Santos and do Nascimento, 2002). This coupled with the fact that molten lead does not have the same enthusiastic (highly reactive) relationship that sodium has with water means that lead fast reactors can be built without an intermediate heat exchanger and therefore lower cost. Besides lead fast reactors (LFRs), lead-cooled accelerator driven systems (ADS) (Abderrahim, 2004) and material test beds (Mamtimin et al., 2018) are both planned. The latter systems will also be used for material validation of other GEN-IV technologies, primarily molten salt and liquid metal fast breeder reactors, as well as pilot studies into the transmutation of spent fuel.

Lead is an ideal coolant in fast systems because it has high atomic mass and low neutron capture cross section, contributing greatly to preserving the neutron flux in fast systems. As the name implies, LFRs utilize a fast neutron flux to breed and burn fuel. ADS and test beds are sub-critical multiplying systems coupled to linear accelerators. Thus, all envisioned systems will make use of a fast fission spectrum, with the ADS and test beds spectrum reaching even higher neutron energies. Unfortunately, no LFR or similar system exists currently which may be used to test lead neutron evaluations. Instead, systems analogous to LFRs need to be used for nuclear data validation. To this end, integral critical and shielding experiments from the International Criticality Safety Benchmark Evaluation Project (ICSBEP) (Anon, 2020) and quasi-differential scattering measurements from Rensselaer Polytechnic Institute (RPI) (Saglime et al., 2010) were identified as lead-sensitive validation systems to use. Critical experiments in the ICSBEP are historical experiments from both the US and former soviet union

(Zrondnikov et al., 2000). Previous work in analyzing these systems by der Marck et al. (2012) and Youmans et al. (2015) suggested that lead cross sections in widely used international nuclear data libraries were deficient in reproducing effective multiplication factors and measured scattering rates. As lead nuclei cross sections are dominated by the scattering reactions, the quasi-differential scattering measurements are helpful in identifying poor scattering cross sections. Furthermore, all but two critical configurations in the ICSBEP are lead-reflected meaning that the differences in k_{eff} between libraries observed by van der Marck could be attributable to scattering as well. To determine the root cause of these issues, MCNPv6.2® (Werner, 2017)[1] was used to simulate the lead-sensitive systems with lead nuclear data from the JENDL-5.0 (Iwamoto et al., 2020), JEFF-3.3 (Plompen et al., 2020), and ENDF/B-VIII.0 (Brown et al., 2018) libraries. Comparisons of the evaluated nuclear data were made as were studies into the relative sensitives of the experiments to the isotopic cross sections. These two steps form the pre-evaluation phase covered in Section 2. Following the pre-evaluation phase, the identified isotopes and reaction cross sections were updated using the Bayesian R-matrix code SAMMY (Larson, 2008) described in Section 3. In addition to the RRR parameters, nuclear data covariance of the evaluated parameters were generated during the Bayesian analysis in Section 4. Finally, the same lead-sensitive systems were simulated again to study the impact the new RRR parameter evaluations made. As the evaluation was sponsored by the DOE-NEUP (Danon et al., 2019), the goal was to produce evaluations that improves fast benchmarks (fast critical experiments, shielding benchmarks, and quasi-differential scattering) over the ENDF/B-VIII.0 library.

2. Pre-evaluation methods

To begin the pre-evaluation phase, MCNP input decks of the lead-sensitive systems (shielding, critical, and quasi-differential measurements) were assembled and run. All calculations made use of ENDF/B-VIII.0 cross sections except for the lead isotopes. Fig. 1 shows the calculated over experimental (C/E) value of k_{eff} from the various libraries for critical benchmarks PMI-04, MMF-06, HMF-64, HMF-57, HMF-27, and PMF-35 (Lell et al., 2020)(Rozhikhin et al., 2020)(Lyutov et al., 2020)(Lee et al., 2020)(Gorbatenko et al., 2020a)(Gorbatenko et al., 2020b).

Simulations using JEFF-3.3 and JENDL-5.0 cross sections calculate similarly for the fast systems shown while the ENDF/B-VIII.0 library performs poorer. In short, there is no good agreement with the experimental values as simulations using any library seem to calculate k_{eff} outside of the reported benchmark error. Since simulating using cross sections from JEFF-3.3 and JENDL-5.0 give similar results, an effort was made to determine which cross sections were causing the differences.

2.1. Differential data for evaluation

The natural isotopes of lead are ^{204}Pb (a/o = 1.4%), ^{206}Pb (a/o = 24.1%), ^{207}Pb (a/o = 22.1%), and ^{208}Pb (a/o = 52.4%) (Prohaska et al., 2022). Lead nuclei are unique among heavy isotopes since they are either double magic (^{208}Pb) or close to double magic (^{206}Pb, ^{207}Pb) nuclei. Double magic refers to both the neutron and proton shells being full. The result of having filled or nearly filled proton and neutron shells is low capture cross sections that are accompanied by large level spacing and high inelastic thresholds. Therefore, elastic scattering, and
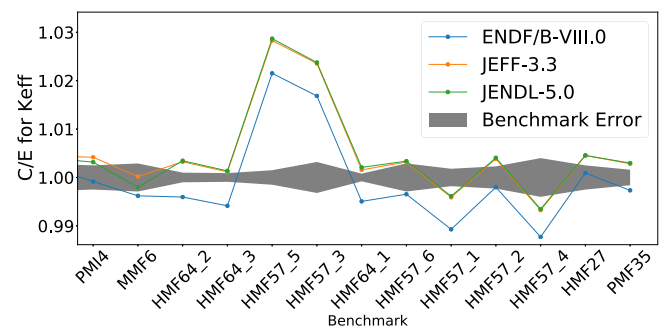

Fig. 1. Collection of C/E values for k_{eff} of fast critical benchmark from the ICSBEP handbook. Simulations from various lead libraries show JEFF-3.3 and JENDL-5.0 out perform ENDF/B-VIII.0 but no library calculates within benchmark uncertainty. All calculations use ENDF/B-VIII.0 fissile and structural materials.

to a smaller extent inelastic, dominates within the resolved resonance region. To summarize the libraries, JEFF-3.3 and JENDL-5.0 evaluated nuclear data files (ENDF) appear almost identical within the RRR. This includes both the partial cross sections and secondary neutron distributions in the three major isotopes. The ENDF/B-VIII.0 evaluations, on the other hand, do not include the most contemporary (n, γ) measurements from nTOF and Geel for ^{206,207}Pb (Borella et al., 2007; Domingo-Pardo et al., 2007, 2006) and have roughly twice the capture worth relative to JENDL/JEFF ^{208}Pb. Additionally, the ENDF/B-VIII.0 evaluations were released before the inelastic data of Mihailescu (Mihailescu and Plompen, 2006; Mihailescu et al., 2008) and Negret (Negret et al., 2015) were available, impacting the inelastic cross section of ^{206}Pb and ^{207}Pb. One constant between lead evaluations is the total cross sections. All current evaluations of ^{206,207,208}Pb derive their total cross sections from transmission measurements done at the Oak Ridge Linear Accelerator (ORELA) in the 1980s by Horen (Horen et al., 1979, 1978), Harvey (Harvey), and Carlton (Carlton et al., 1991).

Though the capture cross sections differ for ^{208}Pb by a factor of two, the elastic-to-capture ratio is on the order of hundreds to thousands. That is to say, the total, and by extension, the integrated elastic cross sections of ^{208}Pb, are consistent between all evaluations. With only the elastic and capture channels open within the ^{208}Pb RRR, the elastic scattering angular distributions (ESAD) cause the majority of the differences in the evaluations. This is not the case with ^{206,207}Pb where inelastic cross sections are present and the probability to absorb neutrons is greater. Summarizing the differential constraints, the cross sections of ^{208}Pb are largely fixed in the RRR except for the elastic scattering angular distributions which are still unconstrained. The minor isotopes ^{206}Pb and ^{207}Pb have larger capture cross section but this only affects thermal systems. The differences in the evaluated elastic and inelastic cross sections are larger for ^{206}Pb and ^{207}Pb than ^{208}Pb but the total cross sections are roughly the same across libraries.

2.2. Sensitivity analysis of lead systems

Of the validation systems, the shielding benchmarks are the least sensitive to the lead cross sections. ALARM-TRAN-PB-SHIELD-001 (Miller et al., 2020), performed at the Valduc burst assembly, reports foil activation measurements with uncertainties on the order of 10% making all evaluations fall within uncertainty. Similarly for ALARM-CF-PB-SHIELD-001 (Manturov et al., 2020), no appreciable differences are seen between the evaluations from 20 to 60 cm worth of lead shielding.

Integral critical experiments were studied via the KSEN card built into MCNP. KSEN is a tally option in eigenvalue problems that produces adjoint-based sensitivity coefficients which are the exact derivative of the eigenvalue with respect to a given parameter, P (Favorite, 2018).

$$S_{k_{eff},p} = \frac{\delta k_{eff}}{k_{eff}} \frac{P}{\delta P} \qquad (1)$$

Table 1
Integrated sensitivities (1×10^{-5} to 20 MeV) of three fast critical assemblies to a variety of lead isotopes and their reactions.

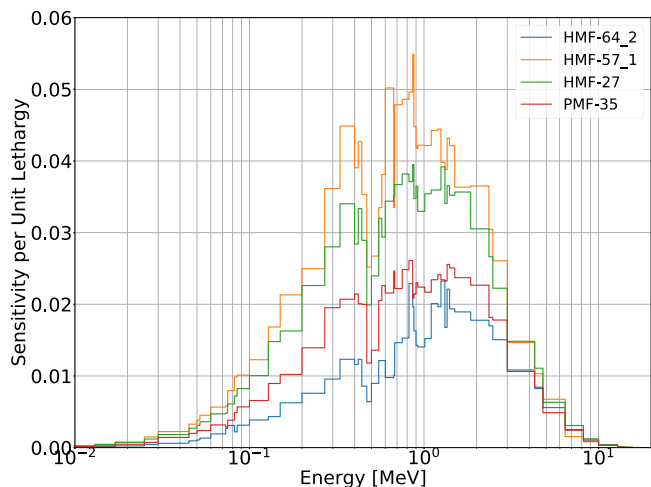| Reaction		PMF-35	HMF-27	HMF-64
^{208}Pb	$(n, el.)$	4.46×10^{-2}	4.14×10^{-2}	1.29×10^{-1}
P_1 Moment		4.81×10^{-2}	4.36×10^{-2}	1.34×10^{-1}
$(n, inl.)$		3.28×10^{-3}	2.06×10^{-3}	4.82×10^{-3}
(n, γ)		-6.37×10^{-6}	-7.37×10^{-6}	-1.54×10^{-4}
^{207}Pb	$(n, el.)$	1.79×10^{-2}	1.68×10^{-2}	5.46×10^{-2}
$(n, inl.)$		4.91×10^{-3}	3.44×10^{-3}	9.75×10^{-3}
(n, γ)		-8.42×10^{-6}	-1.05×10^{-5}	-2.56×10^{-4}
^{206}Pb	(n, el)	1.79×10^{-2}	1.68×10^{-2}	4.97×10^{-2}
$(n, inl.)$		5.21×10^{-3}	3.63×10^{-3}	1.07×10^{-3}
(n, γ)		-1.42×10^{-5}	-1.79×10^{-5}	-4.45×10^{-4}

Fig. 2. Sensitivities of several fast benchmarks to the ^{208}Pb total cross section.

For the analysis here, the sensitivities of k_{eff} with respect to the angle-integrated cross sections and P_1 moment of elastic scattering were calculated using MCNP. As expected from the differential data, elastic scattering is the dominant reaction for all isotopes with the relative contributions being correlated with their natural abundance as shown in Table 1. Since all the fast systems are lead-reflected systems, the sensitivity to the integrated elastic scattering cross section is smaller than the P_1 moment sensitivity. In other words, lead's contribution to k_{eff} for these systems depends solely on its ability to scatter neutrons back into the fissile material. After the elastic scattering reactions, the ^{206}Pb and ^{207}Pb inelastic scattering are the 4th and 5th largest contributors. No sensitivity above 0.001 to any ^{204}Pb cross section is observed and therefore omitted in Table 1.

Besides looking at the sensitivity integrated over all energies, one can plot the sensitivities to a system as a function of energy, Fig. 2. In this way, one can see that for lead-reflected fast critical assemblies, essentially analogs to LFRs, neutrons above 100 keV and below 5 MeV have the most impact. The upper energy limits of the resolved resonance regions for lead in the ENDF/B-VIII.0 are 75 keV for ^{204}Pb, 900 keV for ^{206}Pb, 475 keV for ^{207}Pb, and 1.0 MeV for ^{208}Pb. This results in the RRR of all lead isotopes (except for ^{204}Pb) affecting fast critical systems.

Since the integrated elastic cross sections of ^{208}Pb evaluations are the same for the investigated ENDF (i.e. JEFF-3.3, JENDL-5.0, ENDF/B-VIII.0), one would expect the difference in k_{eff} from ^{208}Pb to be coming entirely from elastic scattering angular distributions. For this reason, a second batch of simulations were run that swapped the ^{208}Pb from ENDF/B-VIII.0 with that of JENDL-5.0, Fig. 3. The impact of switching the ^{208}Pb isotope is dramatic, as the under-prediction of ENDF/B-VIII.0 is completely eliminated and now the critical experiments appear high. Since the main difference between JENDL-5.0 and
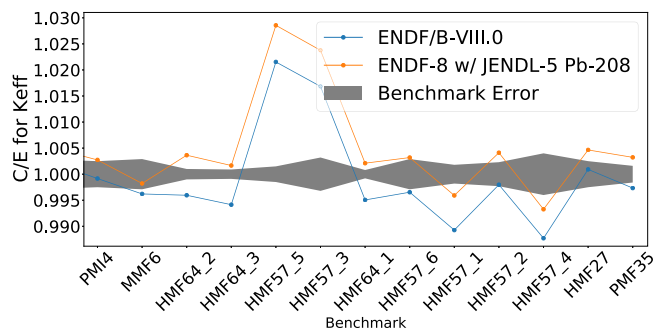

Fig. 3. Calculation of fast benchmarks with ENDF/B-VIII.0 and ENDF/B-VIII.0 with the ^{208}Pb ENDF replaced for JENDL-5.0's version.

ENDF/B-VIII.0's ^{208}Pb is the ESAD, the quasi-differential scattering data was leveraged to see if any additional insights could be gained.

Quasi-differential scattering with the High Energy Scattering System (HESS) at RPI (Saglime et al., 2010) are used to measure the neutron scattering rates from 3 cm and 5 cm long, 3 cm diameter cylinders of natural lead. Eight detectors were spread between 30° and 150° relative to the incident neutron beam record the scattering in 5 ns time-of-flight bins. Using a 30.1 m flight path and relativistic equations for time-of-flight, the experiment can yield counts from 0.5 to 20 MeV. To normalize the simulation to the data, a carbon sample is used which since the scattering of carbon is well-known. On average the carbon normalization is a 6% uncertainty that is applied on top of the systematic and statistical uncertainties (Saglime et al., 2010).

It was seen in both the evaluated nuclear data files of ^{208}Pb and quasi-differential simulations, that the ENDF/B-VIII.0 ^{208}Pb evaluation favors forward scattering. This much forward scattering is not evident in any experimental data, results in too much leakage in fast systems, and is a major contributor to the under-prediction of k_{eff}. With the ESAD of ^{208}Pb determined to be a key issue, the Blatt–Biedenharn (BB) formalism was used to replace the MF-4, MT-2 (scattering angular distributions) in all ENDF/B-VIII.0 lead evaluations (including ^{204}Pb elastic scattering). The Blatt–Biedenharn formalism defines the double differential scattering cross section as a summation of Legendre polynomials dependent on scattering angle, μ, and channel coefficients $B_{Lcc'}$ based on resonance parameters. Full derivation of Eq. (2), can be found in Blatt and Biedenharn original paper (Blatt and Biedenharn, 1952).

$$\frac{\delta\sigma_s}{\delta\Omega} = \sum B_{Lcc'}(E) P_L(\cos(\beta)) \tag{2}$$

In essence, the Blatt–Biedenharn (BB) formalism replaces scattering distributions generated from fast region reaction models (Moldauer, 1963) with those derived from resonance parameters. Changing any one of the resonance parameters (energy, neutron width, orbital angular momentum, total angular momentum) will impact the calculated scattering distribution. Furthermore, the scattering distributions from BB will fluctuate much more rapidly over a given energy range than the fast region reaction models. Calculating the BB version of the ESAD was done by using a modified version of NJOY (Kahler et al., 2019). It is important to note that enabling this function with the RECONR module will break NJOY's ability to properly create ACE files so two versions of NJOY, one with and without BB, is recommended. Formation of the ENDF was done by running the resonance parameters through the BB version of NJOY and then copying and pasting the MF-4, MT-2 from the PENDF into a new ENDF. This ENDF, with new scattering distributions, is processed through a regular version of NJOY to produce an ACE file used in the MCNP simulations.

The effect of the BB treatment on scattering simulations is shown in Fig. 4. First, updating all the elastic scattering distributions within the resolved resonance region allows for better reconstruction of the
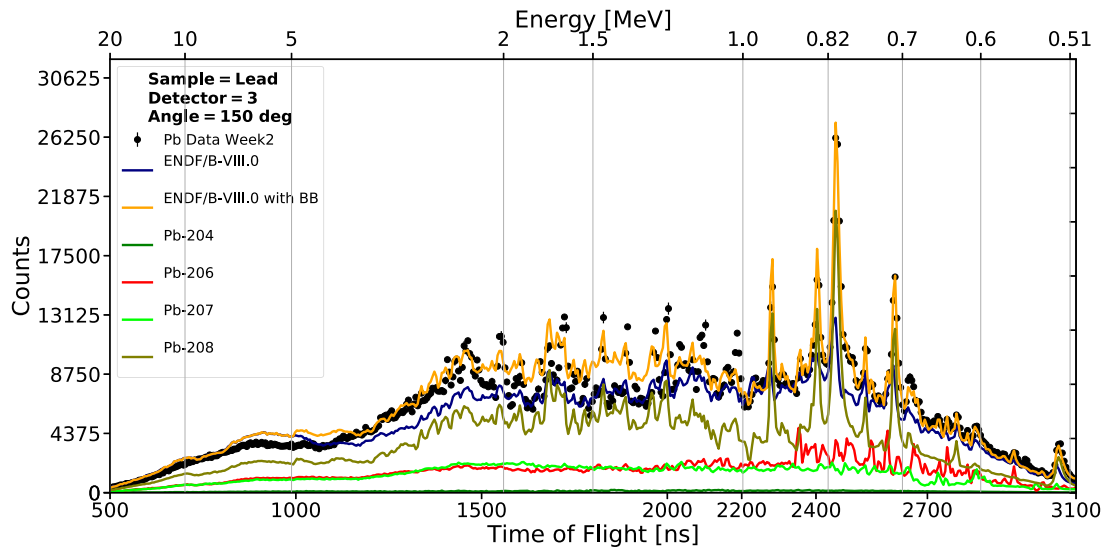
Fig. 4. Experimental neutron scattering counts at the 150° detector from the 3 cm long natural lead sample obtained during week two of measurements. Simulations show the relative contribution and improvement from Blatt–Biedenharn.

scattering counts observed from the experiment below 1 MeV. This was not previously done with the ENDF/B-VIII.0 or any other current library as the ESAD does not fluctuate with energy at small enough intervals to represent the scattering of ^{208}Pb resonances. Secondly, most of the anisotropy observed below 2 MeV is attributable to ^{208}Pb. As noted earlier, the Blatt–Biedenharn formalism relies on knowing the spin and magnitude of resonance widths. Thus, for the resolved resonance region evaluations, updating both the radiation (capture) and neutron (elastic) widths is essential for not only a well defined integrated cross sections but also accurate elastic scattering angular distributions.

3. Evaluations

For the evaluations performed here, the Reich–Moore formalism of the R-matrix was used (LRF=3 in ENDF-6 format Herman and Trkov (2010)). This format enables parameterization of observed resonances with energies, neutron widths, and radiation widths ($E_{res}, \Gamma_n, \Gamma_\gamma$). Additionally, an external part of the R-matrix is included and accounts for scattering radii (potential scattering), bound, and distant levels. Fitting of transmission and capture yield data was performed in the Bayesian R-matrix code SAMMY (Larson, 2008). As the R-matrix requires consistency between the scattering radius, bound levels, distant levels, and observable resonances, it was necessary to update all portions of the RRR. Specifically, the ^{206,207,208}Pb isotopes were examined as they make up the majority of natural lead and possess resolved resonances which directly affect fast systems. The resolution broadening parameters for ORELA transmission data sets were obtained from previous literature by D. Larson (Larson et al., 1984). The capture yield broadening parameters were provided with their corresponding data sets (Borella et al., 2007; Domingo-Pardo et al., 2007, 2006).

3.1. Pb-208

As mentioned earlier, the total cross section of ^{208}Pb is well constrained by the high resolution transmission data from Carlton (Carlton et al., 1991). Likewise, the capture cross section of this nucleus is extremely small, on the level of micro barns. Furthermore, there are only 70 resonances in the RRR of ^{208}Pb from thermal to 1.0 MeV. Most are well isolated so the interference with the potential scattering reveals information about the resonances' spins. All of this is to say that the neutron widths and spins of resonances are available in current evaluations and directly adopted from ENDF/B-VIII.0 in the present work.

Radiation widths have more ambiguity in their magnitudes since no continuous energy differential capture yield measurements exist. Instead, average radiation widths, $\overline{\Gamma_\gamma}$, are used to represent the capture cross section. One way to constrain the radiation widths is with Maxwellian-Averaged Cross Sections (MACS). MACS are the integral averaged capture cross section produced by weighting the capture cross section with a Maxwellian spectrum at a given temperature: (shown in Eq. (3)), k is the Boltzmann constant (8.61 ×10^{-5} eV/K), T is the temperature in Kelvin, m_1 and m_2 are atomic masses in amu of the neutron and target nucleus.

$$\sigma_{mxw}(kT) = \frac{2}{\sqrt{\pi}} \frac{(\frac{m_2}{m_1+m_2})^2}{(kT)^2} \int_0^\infty \sigma_\gamma(E) E \exp\left(\frac{-Em_2}{kT(m_1+m_2)}\right) dE \quad (3)$$

The Karlsruhe Astrophysical Database of Nucleosynthesis in Stars (KADoNIS), estimated the MACS of all isotopes for a variety of stellar temperatures which is applied to studying isotope production in stars. For the MACS(30 keV), KADoNIS reports an average quantity of 0.35 mb for ^{208}Pb. This is close to the values of the JEFF-3.3 and JENDL-5.0 evaluations, but half that of the ENDF/B-VIII.0 evaluation. After consulting several activation measurements from EXFOR by Beer et al. (2003), Ratzel et al. (2004), Weissman et al. (2017), and Macklin and Gibbons (1969) it was concluded that the average radiation width should be halved relative to ENDF/B-VIII.0. Additionally, a direct capture (DC) component was included to increase the capture cross section in between resonances. The representation presented by Beer, shown in Eq. (4), is used as a background cross section in MF-3, MT-102. The direct capture cross section, σ_{DC}, is given in barn and the energy, E, is given in keV as shown in Eq. (4).

$$\sigma_{DC} = 1.798 \times 10^{-5} \sqrt{E} \quad (4)$$

The combined affects of halving the radiation width and adding the DC contribution increases the capture cross section outside of resonances by an order of magnitude between 1 eV - 120 keV but overall reduces the capture worth of ^{208}Pb by a factor of two relative to ENDF/B-VIII.0. A comparison of the MACS from ENDF/B-VIII.0 and new ^{208}Pb evaluation is shown with experimental points from the literature shown in Fig. 5.

Apart from the data set from Macklin, the new evaluation aligns with all Maxwellian points. The reason for all the experimental data sets decreasing at energies above 60 keV is a result of the incident energy reaching the Maxwellian energy multiplied by the reduced mass of the system ($E \geq \frac{kT(m_1+m_2)}{m_2}$). This makes the contribution to the MACS drop
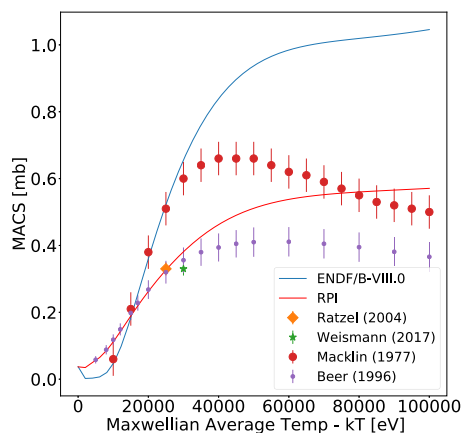
Fig. 5. Maxwellian Averaged Cross Sections (MACS) for the new ^{208}Pb evaluation compared to ENDF/B-VIII.0 and literature values.

Fig. 6. Transmission fitting for RRR extension of ^{208}Pb: 1.0–1.2 MeV.

Fig. 7. Transmission fitting for RRR extension of ^{208}Pb: 1.2–1.4 MeV.

Fig. 8. Capture Yield fitting for ^{206}Pb to Borella data, missing resonance in ENDF/B-VIII.0 library at 59 keV and too large Γ_γ at 64 keV.

off exponentially. The reason the evaluated MACS does not drop off in the plots is because the resonances of lead extend to hundreds of keV.

With the adjustments to the radiation width from MACS and adopting the neutron widths of the ENDF/B-VIII.0, the resonance parameters below 1 MeV are finalized. At this point, the goal of the ^{208}Pb evaluation was to extend the resolved resonance region past 1.0 MeV in order to determine new resonances and the ESAD with which to address the poor scattering simulations between 1.0 and 2.0 MeV.

Extension of the ^{208}Pb RRR was performed with the same Carlton data (Carlton et al., 1991) below 1.0 MeV. Due to the limited resolution of the data, parameterization of resonances could only be accomplished up to 1.5 MeV. Above this energy, resonances start to overlap and could no longer be resolved. Even between 1.0 and 1.5 MeV, there are several resonance spins that could not immediately be determined because the underlying transmission data was insensitive to spin. To overcome this, an automation procedure was developed using SAMMY transmission fitting, MCNP simulations of quasi-differential data, and NJOY (Brain, 2023). Essentially the procedure is to sample all available resonance spins and fit them sequentially through the transmission and scattering data. Combining the quasi-differential data with transmission provides additional spin sensitivity to the fitting procedure that transmission does not possess on its own. This ESAD Automation, enabled resonance parameters to be fit that replicate both the transmission and scattering data well. After all spins were finalized, a final SAMMY solve run was performed to minimize the resonance interference effects. Figs. 6 and 7 show the finalized transmission fit and Appendix lists the new resonance parameters. Constraining the capture cross section remains a challenge for these resonances as there are no capture yields available. The only fix available was to use an average radiation width tuned to the integrated capture cross section equal to the integrated MF-3 MT-102 that existed prior to the RRR extension. Because this normalization is rather arbitrary and there is no differential data to back it up, a 30% uncertainty was applied for the capture covariance. Again the capture cross section is so small that it is not appreciable in systems. After the RRR extension, all resonances were fed in through the BB treatment in NJOY to gain new ESAD, the impact of which will be discussed later.

3.2. Pb-206

The major change required for ^{206}Pb is the incorporation of high fidelity capture data made available after the release of ENDF/B-VIII.0. There are two such measurements: CERN-nTOF by Domingo-Pardo et al. (2007) and JRC Geel by A. Borella (2007) (Borella et al., 2007). In addition to these capture measurements, ORELA transmission by D. J. Horen (1979) (Horen et al., 1979) is used to constrain the total cross section and resonance spin assignments. Of the three measurements,
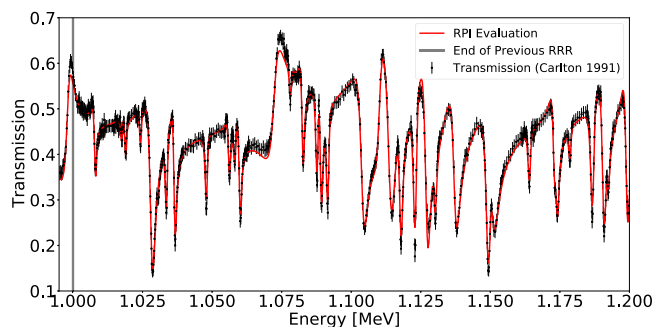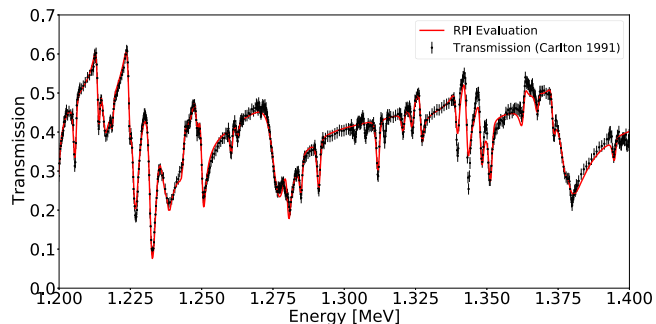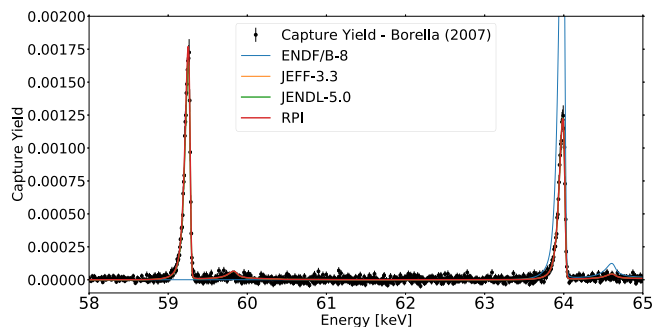
the capture cross sections can be determined reliably below 600 keV and total cross section out to 900 keV.

Fitting capture yield data using SAMMY follows the same process as transmission data. Providing the proper resolution function as well as sample size and thickness are all important since gamma attenuation from the lead sample is an issue. The EXFOR entry for Domingo-Pardo provides the resolution function for the nTOF spectrometer while Borella's thesis (Borella et al., 2005) held values for the Geel setup. Using a resolution function representative of the spectrometer at Geel, SAMMY performs multiple scattering corrections using a finite slab approximation. Base resonance parameters for the Bayesian updating were taken from ENDFB-VIII.0 which has resonances up to 900 keV. The capture yield from different evaluations are shown in Fig. 8.

The resonance at 64 keV is over predicted and the one at 59 keV is entirely missing in the ENDF/B-VIII.0 evaluation. Similar missing or over predicted resonances in the ENDF/B are noticeable in both Borella and Domingo-Pardo sets. In all, around 50 p- and d- wave resonances were identified in the experimental data that were missing from the evaluation. As these resonances are quite small and cannot be observed in transmission experiments, the effects on fast systems

Table 2
SAMMY reduced chi-square of evaluations relative to each differential experiment for Pb-206. Alongside each reduced chi-square is a summed chi-square across all experiments.

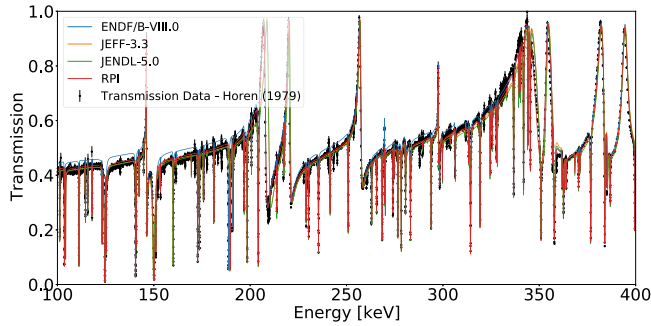| Evaluations	Experiments				
	Domingo capture [400 eV–975 keV]	Borella capture [3–621 keV]	Horen trans. [70–960 keV]	Horen trans. [3–70 keV]	Sum
ENDF/B-VIII.0	3.94	12.4	82.1	4.32	102.8
JEFF-3.3	3.87	1.93	124.67	1.77	132.2
JENDL-5.0	3.87	1.93	124.67	1.77	132.2
RPI	3.85	1.61	32.6	2.76	40.9

Fig. 9. Horen transmission measurement (Horen et al., 1979) fitting in SAMMY for ^{206}Pb: 100 to 400 keV.

Fig. 10. Horen transmission measurement (Horen et al., 1979) fitting in SAMMY for ^{206}Pb: 400 to 900 keV.
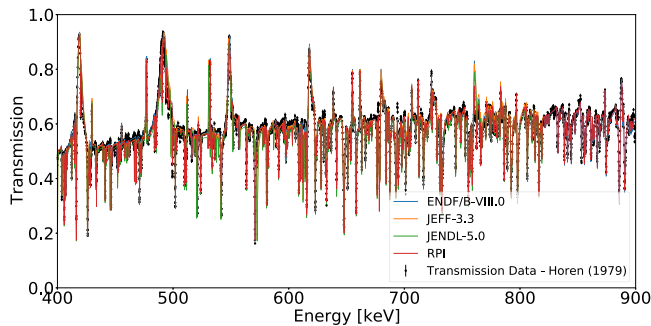

Fig. 11. Horen transmission measurement (Horen et al., 1979) fitting in SAMMY for ^{207}Pb: 640 to 670 keV.

are minor, if not negligible. Still, these resonances will be included in the Blatt–Biedenharn calculations for ESAD at the end so having the most accurate list of parameters will in theory yield the most accurate scattering distributions. Updates to the neutron widths and scattering radius were achieved after incorporating transmission data from Horen et al. (1979). Figs. 9 and 10 show the transmission reconstruction between the newest and contemporary evaluations.

The effective scattering radius is increased from 9.5 fm to 9.7 fm. This causes the lower transmission visible in the earlier energies of Fig. 9.

Due to the high level density of the ^{206}Pb nucleus relative to ^{208}Pb, visually inspecting resonances fits is not practical. Instead, Table 2 summarizes the evaluations reduced χ^2 to all the included differential data calculated from Eq. (5).

$$\chi^2 = \frac{1}{N-1} \sum_{i=0}^{N} \frac{(\sigma_{exp,i} - \sigma_{theory})^2}{\delta^2_{\sigma_{exp,i}}} \quad (5)$$

Here, N is the number of data points for cross section data, σ_{exp} and σ_{theory} are the experimental and theoretical quantities respectively, and $\delta_{\sigma_{exp}}$ is the experimental uncertainty. The poor fits to the transmission data from both JEFF-3.3 and JENDL-5.0 arises from a 1–2 keV energy shift that is apparent in both evaluations. In a practical sense, the neutron and radiation widths, and by extension the cross section, are comparable to the RPI evaluation.
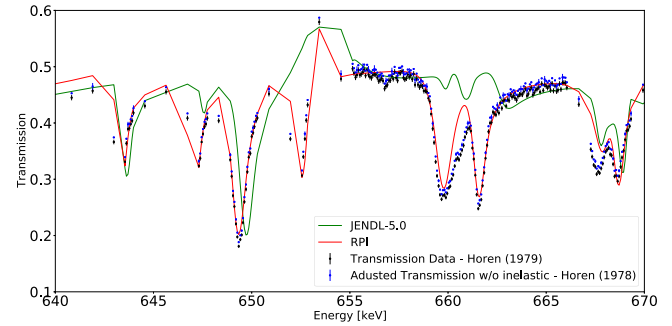
3.3. Pb-207

Evaluating ^{207}Pb required performing Bayesian updating of resonance parameters in the same manner previously shown with ^{206}Pb. For differential data, there is a capture yield measurement by Domingo-Pardo et al. (2006) and ORELA transmission measurement by Horen et al. (1978). Comparing the available parameter files from current evaluations, both JEFF-3.3 and JENDL-5.0 have resonance parameters up to 675 keV. The ENDF/B-VIII.0 evlauation chooses to stop at 475 keV, roughly where the inelastic threshold begins. Looking at the transmission of the JENDL-5.0 library reconstructed from SAMMY, it appeared that the parameters themselves perform well below 650 keV. However, at higher energies the inelastic portion of the cross section does need to be accounted for. The approach here was to use LRF=3 format in the evaluation file and include the inelastic cross section as a background in MF-3. To go about this, a CoH-3 calculation (Kawano, 2016) was used to model the inelastic cross sections. Validation of the fast energy reaction model was performed with differential inelastic gamma production, transmission, and double-differential scattering data and deemed acceptable (Brain, 2023). The inelastic cross section from this calculation was then subtracted off the total cross section reported by Horen and this quantity was inverted to transmission from which SAMMY can fit. For the purposes of nuclear data covariance, the inelastic channel is handled in the ENDF MF-33 whereas the elastic and capture for the RRR are held in ENDF MF-32. Fig. 11 shows the effect of the inelastic cross section in the fitting of the higher end of the RRR. Typically, only the peaks of the resonance (corresponding to the bottom of transmission) are affected since these are the largest cross sections. Again, in Fig. 11, one can see the energy shift relative to the Horen data that is present in the JENDL-5.0/JEFF-3.3 evaluations.

The transmission fits are depicted in Figs. 12 and 13. The RPI evaluation decreased the scattering radius from 9.75 fm in JEFF-3.3 to the 9.70 fm used in ENDF/B-VIII.0.

At 475 keV in Fig. 13, the ENDF/B-VIII.0 RRR evaluation ends and is replaced in the evaluation as a point-wise cross section. Resonance interference effects between 550 and 600 keV seem to be an issue with all evaluations as the transmission between resonances is not reproduced.
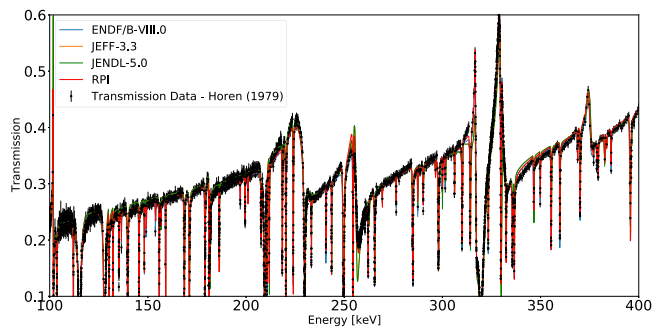
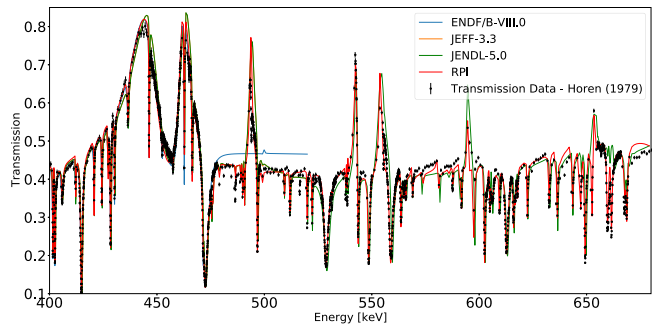**Fig. 12.** Horen transmission measurement (Horen et al., 1979) fitting in SAMMY for ^{207}Pb: 100 to 400 keV.

Fig. 13. Horen transmission measurement (Horen et al., 1979) fitting in SAMMY for ^{207}Pb: 100 to 400 keV.
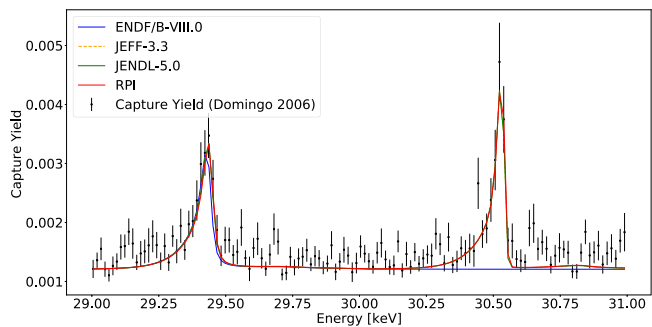

Fig. 14. Domingo-Pardo capture yield (Domingo-Pardo et al., 2006) fitting in SAMMY: 29 to 31 keV.

Looking at the capture yield from Domingo-Pardo, the reported data is not as complete as the ^{206}Pb. This is a feature of an energy dependent background that could not be removed during the reduction of the data. SAMMY was used to fit a constant background to each of the fifteen regions presented in EXFOR. Resonances are reported in 15 energy windows spread from 3 keV to 335 keV. Of the largest capture resonances observed, there is good agreement in the radiation width between all evaluations. Fig. 14 shows an example of the capture yield from Domingo-Pardo data. For some of the smaller resonances observed in the measurement, ENDF/B-VIII.0 does not have a record of them. There is good agreement between the RPI, JEFF-3.3, and JENDL-5.0 evaluations at both the 29.4 keV and 30.5 keV resonances. ENDF/B-VIII.0 matches the 29.4 keV but does not have the 30.5 keV resonance.

Overall, very little adjustment is done to the capture cross sections after adopting the JEFF-3.3 resonance parameters. It was necessary to perform an energy shift of all the resonances from those used in JEFF-3.3 back to the Horen values reported believed to be correct. The energy shift of resonances distorts the SAMMY reduced chi-square

Table 3

SAMMY reduced chi-square of evaluations relative to each differential experiment for Pb-207. Alongside each reduced chi-square is a summed chi-square across all experiments.

Evaluation	Experiments		
	Domingo capture [3–300 keV]	Horen trans. [15–475 keV]	Sum
ENDF/B-VIII.0	57.77	19.82	77.59
JEFF-3.3	43.53	62.34	111.9
JENDL-5.0	43.15	62.34	105.5
RPI	41.50	17.32	58.82

in Table 3 for JEFF-3.3/JENDL-5.0 relative to the Horen data. The actual neutron and radiation widths for these evaluations are capable of reproducing the differential measurements well, on par with the RPI evaluation. Furthermore, the RPI, JEFF-3.3, and JENDL-5.0 libraries have resonances past the 475 keV upper limit of ENDF/B-VIII.0, so if anything, the ENDF/B-VIII.0 evaluation offers the greatest opportunity for improvement.

With all differential data fit using SAMMY, the new resonance parameters were used to calculate the elastic scattering distributions via the Blatt–Biedenharn version of NJOY for all isotopes. Besides updating both resonance parameters (MF-2) and elastic scattering angular distribution (MF-4 MT-2), the resolved resonance region evaluation performed through the Bayesian framework of SAMMY provided new nuclear data covariance.

4. Covariance

Nuclear data covariance were calculated for the major reaction channels present in the respective RRRs. With the Bayesian process formulated in SAMMY, direct uncertainties for all resonance parameters are calculated simultaneously from the fitting procedure. Thus, resonance parameter uncertainties (MF-32) can be directly calculated and put into the evaluation files. However, before the MF-32 can be inserted into the files, some work regarding the magnitude of the uncertainties needs to be done. The reason for this is because the SAMMY produced MF-32 are generally too small by community guidelines outlined by Smith (2011). Multiple reasons exist for why the covariance are too small, primarily incomplete knowledge of the experimental uncertainties and model deficiencies. For example, the R-matrix does not include direct capture processes but this was included in the ^{208}Pb evaluation. Additionally, the Carlton transmission data (Carlton et al., 1991) does not provide information regarding systematic uncertainties. Both of these will mean the uncertainties in MF-32 are too small. In either case, multiplying the covariance by the SAMMY variance from the reduced χ^2 calculation brings the uncertainties to "acceptable" values. These acceptable values are laid out in ENDF-377 which state that uncertainties cannot be below the neutron standards for that reaction type (Smith, 2011). For scattering reactions hydrogen is the standard and generally shows uncertainties of 1%. Therefore the χ^2 multiplier fixes the resonance portion of the RRR by bringing it above that value, but below the first resonance, there is still a lower uncertainty than expected. To address this, a scattering radius uncertainty of 2%–3% was introduced into the MF-32 for specific ℓ states of the different lead nuclei. This is inline with reported uncertainties from Sears (Sears, 1962) shown in Table 4 and typically only the $\ell = 0$ is provided uncertainties. The outcome of scattering radius uncertainty is to act as a correlated uncertainty that brings the relative uncertainty of the cross section below the first resonance from $\leq 1\%$ to the 2%–3% range as shown in Fig. 15.

With the resonance parameter uncertainties now calculated and the resonances used to calculate the elastic scattering angular distributions, the focus shifted to determining the uncertainty on ESAD from resonance parameters. Unfortunately, while SAMMY can calculate ESAD

Table 4

Scattering radii values and uncertainties for different evaluations. Accepted values are taken from Sears (Sears, 1962).

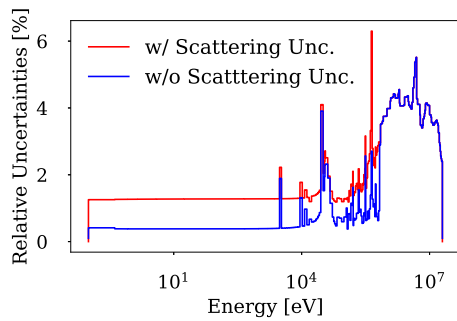| Isotope	Evaluation	R' [fm]
Pb-206	*Accepted*	*9.54(20)*
	ENDF-8	9.50
	JEFF-3.3	9.70
	JENDL-5.0	9.70
	RPI	**9.70 (0.03)**
Pb-207	*Accepted*	*9.57(20)*
	ENDF-8	9.50
	JEFF-3.3	9.55
	JENDL-5.0	9.55
	RPI	**9.55 (0.03)**
Pb-208	*Accepted*	*9.46(12)*
	ENDF-8	9.69
	JEFF-3.3	9.75
	JENDL-5.0	9.75
	RPI	**9.70 (0.03)**

Fig. 15. Relative uncertainty on the total cross section of ^{207}Pb with and without the scattering radius uncertainties. Without scattering radii uncertainties, the total cross section below $E_n \leq 3$ keV has too little uncertainty.

Fig. 16. Relative difference in the uncertainty on the P_1 moment for 200–300 keV as a function of sample history.

Fig. 17. P_1 moment scattering uncertainties for ^{208}Pb.

Fig. 18. Scattering distribution of ^{208}Pb to 90°. ENDF/B-VIII.0 uses a smooth angular distribution from the optical model and the RPI evaluation uses BB below 1.5 MeV.

through BB, it cannot produce the uncertainties on these parameters. Instead, a Monte-Carlo approach was developed to propagate the uncertainties of resonance parameters to the a_1 coefficient through SAMMY. While higher coefficients are supported in the ENDF, only a_1 coefficients uncertainties are supported by NJOY so no other information can be included in the evaluation (Chiba, 2007). Using the resonance parameters (MF-2) and their uncertainties (MF-32), correlated sampling of resonances is performed for the entire RRR. This sampling is used to create hundreds of synthetic instances of the resolved resonance region for the nucleus in question and each one is ran through the Blatt–Biedenharn module in SAMMY. Binning and averaging the scattering distributions of these hundreds of ESADs into 100 keV bins then yield covariance for a_1 coefficients. Studies into the sampling convergence with the number of histories were performed. From these studies it was deemed that roughly 500 instances would provide sufficient convergence with smaller bins requiring more samples. Convergence was defined as a relative difference in bin $\leq$ 1%. Fig. 16 shows the convergence of a representative bin corresponding to 200–300 keV. The calculations performed here were using 1000 sample histories.

The uncertainties calculated with this method also produce uncertainties that are nominally too small because they are below 1%. This is lower than the scattering uncertainty on hydrogen which is a neutron standard you cannot be better than (Smith, 2011). The quasi-differential data was leveraged to find the magnitude of uncertainties on the P_1 moment which recreated uncertainties comparable to the experimental data. This analysis comes with a few caveats, the first that only ^{208}Pb ESAD was perturbed in this study. This is an issue as the experimental data is natural lead, so only ^{208}Pb resonances observed in the natural data can be used. Thus, the contributions from ^{206}Pb and ^{207}Pb are not included and the uncertainties presented here
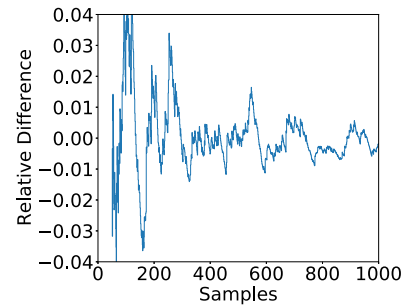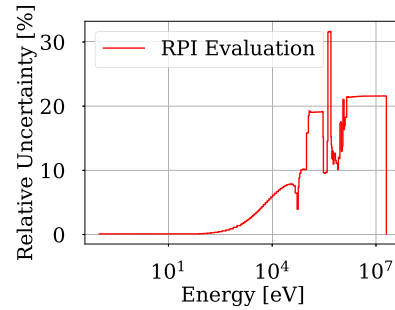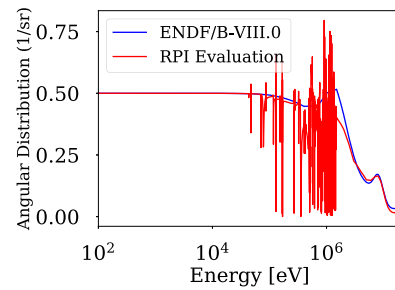
are the upper limit on the P_1 moment. In the end it was determined that 20%–30% uncertainties on the ^{208}Pb ESAD recreated the 6% total uncertainty on the quasi-differential scattering data. The final energy dependent scattering uncertainty (MF-34) for ^{208}Pb is presented in Fig. 17.

Unfortunately, the impact of minor isotopes is less apparent in the natural scattering sample so the same approach was not attempted and no uncertainties on the scattering distributions are given. With the formatting of the covariance into the evaluated nuclear data files, the RRR was concluded.

5. Outcomes

Validation via lead-sensitive systems was performed again on critical experiments and quasi-differential scattering to see the impact of the RRR evaluation. Of the changes brought about with the RRR evaluation, the extension of the resolved resonance region for ^{208}Pb is perhaps the most dramatic. While the total and elastic cross section remains roughly the same as other evaluations, the ability to derive new elastic scattering distributions from Blatt–Biedenharn cannot be understated. Scattering over the large isolated resonances is now taken into account directly instead of the average scattering bins that are computed from
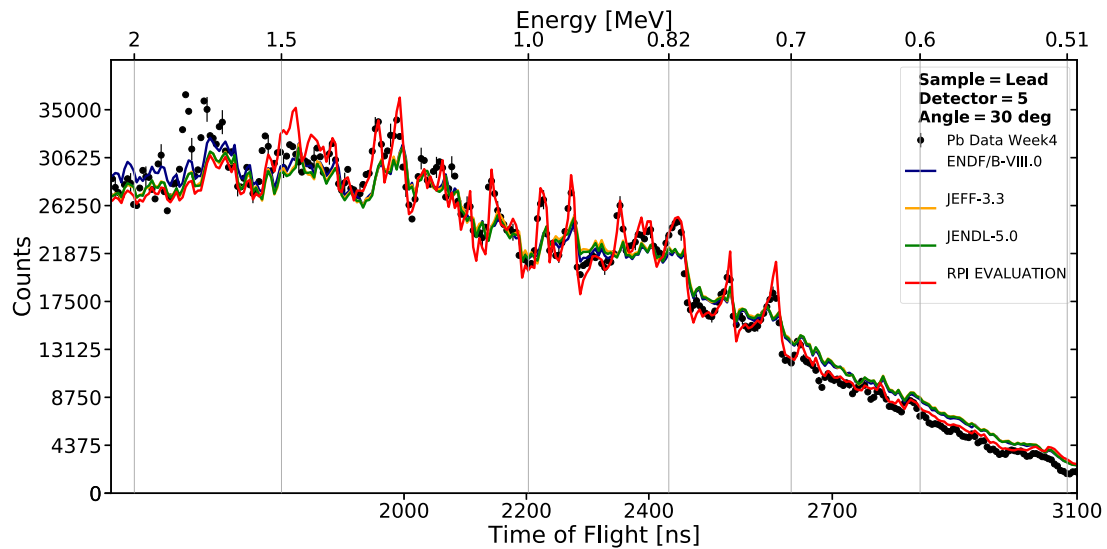
Fig. 19. Simulations of the RPI scattering experiment compared to experimental data for 5 cm thick sample at 30° relative to incident beam.
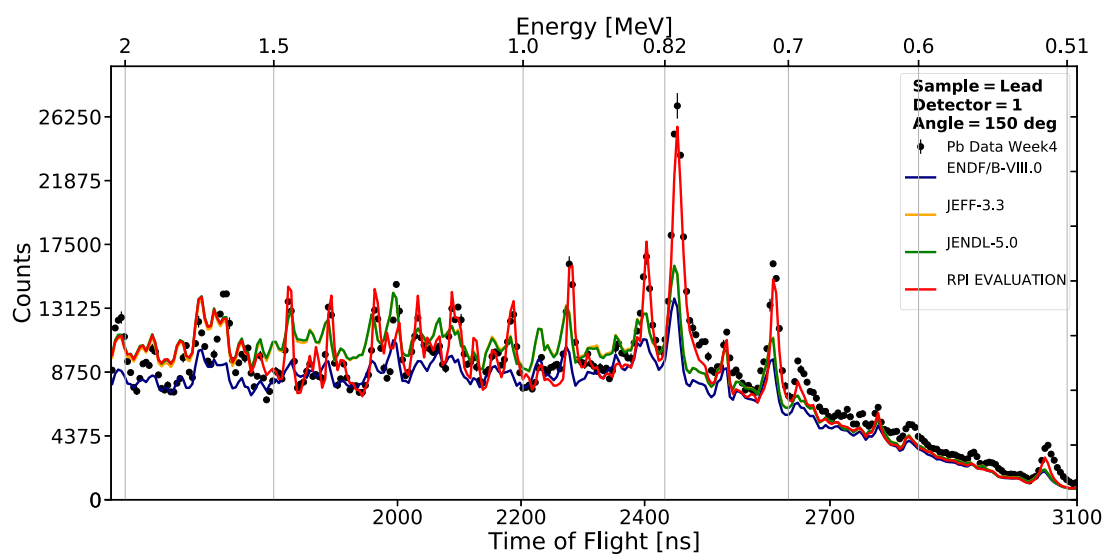

Fig. 20. Simulations of the RPI scattering experiment compared to experimental data for 5 cm thick sample at 150° relative to incident beam.

the fast energy reaction model calculations. Fig. 18 shows the scattering distribution to 90° from the new evaluation compared to ENDF/B-VIII.0. Below 1.5 MeV, the scattering distributions fluctuate more than ENDF/B-VIII.0 to accommodate scattering physics over the resonances.

The impact of the alternative scattering physics is best seen in quasi-differential scattering data. At both the forward and backward scattering angles, the RPI evaluation outperforms all others in predicting the experimental data. Figs. 19 and 20 depict simulations of the scattering experiments with the experimental data below 2 MeV. Up to 1.5 MeV, the RPI evaluation predicts all resonance peaks and scattering fluctuations in natural lead better than the other libraries. After 1.5 MeV, the evaluation matches that of JEFF-3.3/JENDL-5.0 as the cross section and angular distributions are roughly the same. The relative poorer prediction after 1.5 MeV arises from the fact the scattering distributions are now calculated with an optical producing

energy averaged scattering distributions. At energies below 700 keV all evaluations tend to under-predict the back scattering rate. A potential reason could come from incorrect scattering in ^{207}Pb, which has an inelastic component that is handled again with an optical model.

With the improved scattering kernel, there is the assumption that the fast critical benchmarks will also experience better prediction over other libraries. As the new lead evaluations are to be included in the next version of the ENDF/B library, ENDF/B-VIII.1β2, the performance of the entire library was tested. The ENDF/B-VIII.1β2 therefore contains the beta version of updated fissile isotopes, structural isotopes (such as Fe) and lead (with cross sections reworked up to 20 MeV). Fig. 21 shows the final performance of the evaluations against fast critical benchmarks.

For clarification, the lead isotopes also received a new fast region evaluation which will have an effect on the k$_{eff}$ (Brain, 2023). However, most of the improvement for fast systems resulted from MF-4,
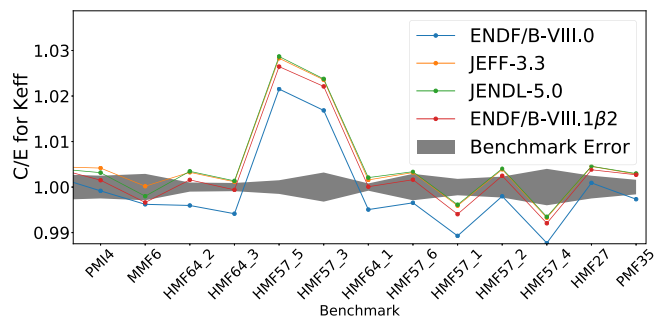
Fig. 21. C/E values for fast integral experiments of ENDF/B-VIII.0, JEFF-3.3, JENDL-5.0, and ENDF/B-VIII.1β2. The latter (ENDF/B-VIII.1β2) contains the new lead evaluations.

Fig. 22. C/E values for fast integral experiments of ENDF/B-VIII.0, JEFF-3.3, JENDL-5.0, and ENDF/B-VIII.1β2. The latter (ENDF/B-VIII.1β2) contains the new lead evaluations.

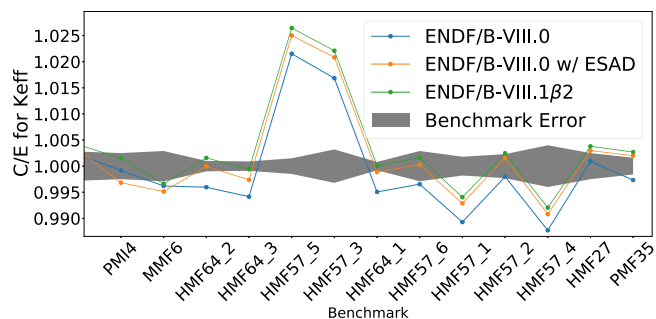MT-2 modifications coming from the RRR evaluations. This is shown in Fig. 22 where three simulations are included: all ENDF/B-VIII.0, ENDF/B-VIII.0 with ESAD from new evaluations, and all ENDF/B-VIII.1β2. For most of the fast benchmarks, just changing the ESAD accounts for 80% of the difference between ENDF/B-VIII.0 and ENDF/B-VIII.1β2 libraries.

Even after all the changes to incorporate better physics some of the benchmarks appear to calculate outside of the experimental uncertainties, specifically HMF-57 cases 3 and 5. Careful analysis of these integral benchmarks was performed and in the end it was determined that the HMF-57 experiment suite should not be considered in fast region evaluations as the multiplication achieved during the experiment was too low for the extrapolation to critical (Brain, 2023). While the other experiment campaigns did reach high enough multiplication for extrapolation to critical, none of the geometries in the ICSBEP ever achieved delayed critical in reality. This is not ideal for nuclear data validation as then some reliance must be made on the extrapolated geometry which may or may not be correct. For this reason, the authors are suggesting to look into revising the benchmark entries in the ICSBEP or performing new lead-reflected fast critical experiments on which to validate the libraries.

6. Conclusion

The resolved resonance region of the three major isotopes of natural lead were re-evaluated under a DOE-NEUP funded project for the purpose of improving the cross sections for lead-cooled fast systems. To this end, the RRRs of ^{206,207,208}Pb were all re-evaluated, which included an extension of the RRR for ^{208}Pb. The end goal of these evaluations were to obtain well characterized resonance parameters to define both integrated cross sections and calculate elastic scattering angular distributions from. This is because elastic scattering appears

to be the dominant reaction for all lead isotopes in the application to fast reactors as observed from sensitivity studies of analogous critical systems. The evaluation process utilized Bayesian fitting in the R-matrix code SAMMY which allowed for not only fitting of experimental data but developing covariance as well. For the first time in an evaluation, the quasi-differential scattering data was leveraged for spin assignments of resonances as well as constraining the P_1 moment uncertainties.

The outcome of the RRR evaluation is an improved natural scattering kernel shown in the simulations of the quasi-differential data. Furthermore with the new ESAD, fast critical systems do see an improvement in C/E over all current libraries. After considerable review of the benchmark geometries it was determined that the 2000+ pcm bias in the HMF-57 cases 3 and 5 is not due to lead but rather the geometry itself. Too low multiplication was obtained for a reliable extrapolation to be performed and in this case it effects all configurations in HMF-57. It is suggested to not use these systems for nuclear data validation and that new experiments be undertaken to replace them in the ICSBEP.

CRediT authorship contribution statement

Peter Brain: Writing – original draft, Formal analysis, Conceptualization. **Yaron Danon:** Investigation, Funding acquisition. **Dave Brown:** Investigation, Funding acquisition. **Devin Barry:** Methodology, Investigation. **Amanda Lewis:** Resources, Methodology. **Tim Trumbull:** Methodology, Investigation. **Toshihiko Kawano:** Methodology, Investigation.

Declaration of competing interest

The authors declare the following financial interests/personal relationships which may be considered as potential competing interests: Peter Brain reports financial support was provided by US Department of Energy. If there are other authors, they declare that they have no known competing financial interests or personal relationships that could have appeared to influence the work reported in this paper.

Data availability

New lead evaluations will be available in ENDF/B-VIII.1 release.

Acknowledgments

Appendix. New Pb-208 resonance parameters

Table A.5

Table A.5
Newly fit resonance parameters of ^{208}Pb above 1.0 MeV and their associated uncertainties.

J^π	L	Energy [eV]	δ_E [eV]	Γ_γ [meV]	δ_{Γ_γ} [meV]	Γ_n [meV]	δ_{Γ_n} [meV]
1.50	2	1.0079e+06	2.1718e+01	1.6600e+02	1.6600e+01	2.4078e+05	1.0397e+04
0.50	0	1.0724e+06	4.3315e+02	1.6598e+02	1.6599e+01	4.6242e+06	9.5090e+04
0.50	0	1.1102e+06	4.3675e+01	1.6600e+02	1.6600e+01	3.1074e+06	1.4765e+05
2.50	2	1.0283e+06	1.3466e+01	1.8601e+02	1.8600e+01	1.5363e+06	2.0810e+04
−3.50	3	1.0335e+06	1.9971e+01	1.8599e+02	1.8599e+01	1.8454e+05	7.6187e+03
2.50	2	1.0365e+06	1.4106e+01	1.8599e+02	1.8599e+01	4.6718e+05	1.2441e+04
−3.50	3	1.0175e+06	2.9693e+01	1.8599e+02	1.8599e+01	4.4761e+04	3.5258e+03
2.50	2	1.0187e+06	3.0188e+01	1.8600e+02	1.8600e+01	9.2208e+04	5.8893e+03
−3.50	3	1.0242e+06	2.9978e+01	1.8597e+02	1.8599e+01	6.3743e+04	4.2867e+03
−2.50	3	1.0479e+06	2.1649e+01	1.8600e+02	1.8600e+01	2.2919e+05	9.1879e+03
1.50	2	1.0560e+06	3.0559e+01	1.8599e+02	1.8600e+01	1.9277e+05	1.1109e+04
−3.50	3	1.0581e+06	3.3913e+01	1.8597e+02	1.8599e+01	7.3767e+04	5.3764e+03
2.50	2	1.0599e+06	1.7626e+01	1.8600e+02	1.8600e+01	3.2938e+05	1.1007e+04
−3.50	3	1.0781e+06	2.8433e+01	1.8600e+00	1.8600e−01	4.5183e+04	3.4411e+03
2.50	2	1.0825e+06	1.6504e+01	1.8600e+00	1.8600e−01	2.5236e+05	8.2296e+03
−3.50	3	1.0877e+06	1.5794e+01	1.8600e+00	1.8600e−01	2.5975e+05	7.4228e+03
2.50	2	1.0890e+06	1.4780e+01	1.8600e+00	1.8600e−01	4.7282e+05	1.2649e+04
−3.50	3	1.0914e+06	1.7696e+01	1.8600e+00	1.8600e−01	2.6902e+05	9.0524e+03
−1.50	1	1.1032e+06	3.1934e+01	1.8600e+00	1.8600e−01	4.0149e+06	9.3853e+04
1.50	2	1.1140e+06	2.6853e+01	1.8600e+00	1.8600e−01	2.6431e+06	6.9236e+04
2.50	2	1.1177e+06	1.7079e+01	1.8600e+00	1.8600e−01	6.3083e+05	1.9007e+04
−3.50	3	1.1229e+06	1.4252e+01	1.8600e+00	1.8600e−01	5.2496e+05	1.1715e+04
2.50	2	1.1272e+06	2.0359e+01	1.8600e+00	1.8600e−01	1.6540e+06	3.4570e+04
−1.50	1	1.1297e+06	3.5246e+01	1.8600e+00	1.8600e−01	7.8497e+05	4.6691e+04
−1.50	1	1.1365e+06	3.3311e+01	1.8600e+00	1.8600e−01	3.3694e+06	8.5824e+04
−3.50	3	1.1492e+06	2.0988e+01	1.8600e+00	1.8600e−01	1.1288e+06	2.3328e+04
−1.50	1	1.1501e+06	5.9215e+01	1.8600e+00	1.8600e−01	3.1865e+06	8.9072e+04
−3.50	3	1.1639e+06	3.1045e+01	1.8600e+00	1.8600e−01	1.4830e+05	7.8020e+03
1.50	2	1.1728e+06	3.4634e+01	1.8600e+00	1.8600e−01	5.1823e+05	3.3963e+04
2.50	2	1.1739e+06	3.2442e+01	1.8600e+00	1.8600e−01	3.9170e+05	2.2799e+04
−3.50	3	1.1785e+06	3.8604e+01	1.8600e+00	1.8600e−01	8.5454e+04	6.0241e+03
−2.50	3	1.1866e+06	1.8296e+01	1.8600e+00	1.8600e−01	5.8163e+05	1.5178e+04
2.50	2	1.1906e+06	1.6467e+01	1.8600e+00	1.8600e−01	9.8644e+05	2.2202e+04
2.50	2	1.1920e+06	4.4252e+01	1.8600e+00	1.8600e−01	1.7406e+05	1.1546e+04
2.50	2	1.1990e+06	1.6309e+01	1.8600e+00	1.8600e−01	7.5125e+05	1.7914e+04
−3.50	3	1.2055e+06	2.3609e+01	1.8600e+00	1.8600e−01	2.4257e+05	9.3804e+03
2.50	2	1.2136e+06	2.2153e+01	1.8600e+00	1.8600e−01	2.8618e+05	1.2156e+04
−0.50	1	1.2149e+06	6.3507e+01	1.8600e+00	1.8600e−01	2.8338e+06	1.1810e+05
−2.50	3	1.2186e+06	4.4930e+01	1.8600e+00	1.8600e−01	1.0755e+05	8.4945e+03
−1.50	1	1.2243e+06	2.3000e+01	1.8600e+00	1.8600e−01	9.0184e+05	6.6018e+04
2.50	2	1.2263e+06	2.3928e+01	1.8600e+00	1.8600e−01	1.6468e+06	4.3326e+04
2.50	2	1.2323e+06	6.1181e+01	1.8600e+00	1.8600e−01	9.6052e+05	6.6945e+04
−3.50	3	1.2326e+06	4.3872e+01	1.8600e+00	1.8600e−01	1.9216e+06	3.6858e+04
−1.50	1	1.2351e+06	8.4838e+01	1.8600e+00	1.8600e−01	6.7177e+06	1.7747e+05
2.50	2	1.2382e+06	6.8285e+01	1.8600e+00	1.8600e−01	1.1901e+05	1.1640e+04
2.50	2	1.2502e+06	2.1555e+01	1.8600e+00	1.8600e−01	8.5914e+05	2.5727e+04
−0.50	1	1.2478e+06	4.7892e+01	1.8600e+00	1.8600e−01	8.2445e+05	5.4160e+04
0.50	0	1.2435e+06	5.6585e+01	1.8600e+00	1.8600e−01	8.8130e+05	6.9899e+04
−2.50	3	1.2603e+06	4.8868e+01	1.8600e+00	1.8600e−01	1.5106e+05	1.0708e+04
−3.50	3	1.2625e+06	3.8427e+01	1.8600e+00	1.8600e−01	6.0806e+04	5.0283e+03
1.50	2	1.2761e+06	4.7231e+01	1.8600e+00	1.8600e−01	5.7148e+06	1.0162e+05
2.50	2	1.2802e+06	3.2321e+01	1.8600e+00	1.8600e−01	5.3783e+05	2.6738e+04
−2.50	3	1.2848e+06	4.4398e+01	1.8600e+00	1.8600e−01	2.8596e+05	1.7610e+04
−2.50	3	1.2910e+06	3.3960e+01	1.8600e+00	1.8600e−01	3.9039e+05	1.8359e+04
−3.50	3	1.3117e+06	3.1356e+01	1.8600e+00	1.8600e−01	2.7687e+05	1.1680e+04
−1.50	1	1.3266e+06	4.0387e+01	1.8600e+00	1.8600e−01	5.5264e+06	3.2027e+04
−2.50	3	1.3206e+06	5.3470e+01	1.8600e+00	1.8600e−01	1.0034e+05	8.2431e+03
−2.50	3	1.3237e+06	5.1214e+01	1.8600e+00	1.8600e−01	1.1076e+05	8.7303e+03
1.50	2	1.3393e+06	3.9665e+01	1.8600e+00	1.8600e−01	3.7670e+05	1.9531e+04
−1.50	1	1.3426e+06	2.8433e+01	1.8600e+00	1.8600e−01	1.2532e+06	4.7337e+04
2.50	2	1.3478e+06	3.0794e+01	1.8600e+00	1.8600e−01	3.5160e+05	1.6563e+04
−3.50	3	1.3511e+06	3.0531e+01	1.8600e+00	1.8600e−01	3.7822e+05	1.5479e+04
−2.50	3	1.3676e+06	5.5092e+01	1.8600e+00	1.8600e−01	8.9839e+04	7.8244e+03
0.50	0	1.3627e+06	6.0114e+01	1.8600e+00	1.8600e−01	5.3360e+05	3.7988e+04
2.50	2	1.3730e+06	4.8175e+01	1.8600e+00	1.8600e−01	1.5623e+06	1.1846e+04
1.50	2	1.3773e+06	6.9104e+01	1.8600e+00	1.8600e−01	4.2334e+06	2.2020e+05
1.50	2	1.3784e+06	9.1159e+01	1.8600e+00	1.8600e−01	4.2460e+06	2.3736e+05
−2.50	3	1.3946e+06	6.9487e+01	1.8600e+00	1.8600e−01	1.4380e+05	1.2936e+04
−3.50	3	1.4062e+06	2.8308e+01	1.8600e+00	1.8600e−01	5.9069e+05	1.9553e+04
2.50	2	1.4113e+06	2.5125e+01	1.8600e+00	1.8600e−01	9.2008e+05	2.7659e+04
1.50	2	1.4239e+06	5.1277e+01	1.8600e+00	1.8600e−01	4.1553e+05	2.8876e+04
−3.50	3	1.4277e+06	2.8342e+01	1.8600e+00	1.8600e−01	8.9886e+05	2.6210e+04
−3.50	3	1.4311e+06	6.1164e+01	1.8600e+00	1.8600e−01	1.5231e+05	1.2041e+04
2.50	2	1.4406e+06	4.5069e+01	1.8600e+00	1.8600e−01	4.7279e+05	2.7721e+04
−3.50	3	1.4411e+06	9.8739e+01	1.8600e+00	1.8600e−01	2.1500e+05	2.0478e+04
−2.50	3	1.4749e+06	5.6515e+01	1.8600e+00	1.8600e−01	5.1734e+06	9.5972e+04
−3.50	3	1.4847e+06	3.0499e+01	1.8600e+00	1.8600e−01	7.6224e+05	2.3609e+04

References

Abderrahim, H., 2004. MYRRHA: A Multipurpose Experimental ADS for R & D objectives. European Particle Accelerator Conference.

Anon, 2020. Int. crit. saf. benchmark eval. project handbook. NEA/NSC/DOC/.

Beer, H., Rochow, W., Käppeler, F., Rauscher, T., 2003. The 208Pb(n,Γ) cross section. Nuclear Phys. A 718, 518–520. http://dx.doi.org/10.1016/S0375-9474(03)00829-7, URL https://www.sciencedirect.com/science/article/pii/S0375947403008297.

Blatt, J.M., Biedenharn, L.C., 1952. The angular distribution of scattering and reaction cross sections. Rev. Modern Phys. 24, 258–272. http://dx.doi.org/10.1103/RevModPhys.24.258, URL https://link.aps.org/doi/10.1103/RevModPhys.24.258.

Borella, A., Gunsing, F., Moxon, M., Schillebeeckx, P., Siegler, P., 2007. High-resolution neutron transmission and capture measurements of the nucleus ^{206}Pb. Phys. Rev. C 76, 014605. http://dx.doi.org/10.1103/PhysRevC.76.014605, URL https://link.aps.org/doi/10.1103/PhysRevC.76.014605.

Borella, A., Schillebeeckx, P., Wynants, R., et al., 2005. The Capture Yield from 3 keV to 620 keV, Total Cross Section and Resonance Parameters of 206-Pb, Fe-56 Capture Cross Sections (Ph.D. thesis). Universiteit Gent.

Brain, P., 2023. Neutron Evaluation and Validation of Natural Lead Isotopes for Fast Spectrum Systems (Ph.D. thesis). Rensselaer Polytechnic Institute, Troy, NY.

Brain, P., Danon, Y., Brown, D., Barry, D., 2023. Resolved Resonance Region analysis of ^{206}Pb, ^{207}Pb, ^{208}Pb for next generation lead-cooled fast systems. EPJ Web Conf. 284.

Brown, D.A., et al., 2018. ENDF/B-VIII.0: the 8th major release of the nuclear reaction data library with cielo-project cross sections, new standards and thermal scattering data. Nucl. Data Sheets 148.

Carlton, R.F., Winters, R.R., Harvey, J.A., Hill, N.W., 1991. R-matrix analysis of an ORELA measurement of n+208Pb total cross section from 78 to 1700 kev. J. Bull. Am. Phys. Soc. Ser. II 36, 1349 (J10–10).

Chiba, S., 2007. ERRORJ: A code to process neutron-nuclide reaction cross section covariance, version 2.3. Reactor Phys. Anal. Eval. Group, Adv. Nucl. Syst. Res. Dev. Directorate.

Danon, Y., Brown, D., et al., 2019. Improvements of Nuclear Data Evaluations for Lead Isotopes in Support of Next Generation Lead-cooled Fast Systems. Tech. rep., DOE-NEUP MS-NE-2, DOE Technical Narrative 19-16739.

Domingo-Pardo, C., Abbondanno, U., Aerts, G., Álvarez, H., Alvarez-Velarde, et al., 2007. Measurement of the radiative neutron capture cross section of ^{206}Pb and its astrophysical implications. Phys. Rev. C 76, 045805. http://dx.doi.org/10.1103/PhysRevC.76.045805, URL https://link.aps.org/doi/10.1103/PhysRevC.76.045805.

Domingo-Pardo, C., Abbondanno, U., Aerts, G., Álvarez-Pol, H., et al., 2006. Resonance capture cross section of ^{207}Pb. Phys. Rev. C 74, 055802. http://dx.doi.org/10.1103/PhysRevC.74.055802, URL https://link.aps.org/doi/10.1103/PhysRevC.74.055802.

Favorite, J.A., 2018. Adjoint-based sensitivity analysis and uncertainty quantification for keff: Using the MCNP ksen card. http://dx.doi.org/10.2172/1467190.

Gorbatenko, M., et al., 2020a. SPHERICAL ASSEMBLY OF 235u(90 HEU-met-FAST-027. Int. Crit. Saf. Benchmark Eval. Project Handb. NEA/NSC/DOC(95)03/II, NEA 7329, OECD Nuclear Energy Agency, Paris.

Gorbatenko, M., et al., 2020b. Spherical assembly of ^{239}pu(δ, 98 reflector: PU-MET-Fast-035. Int. Crit. Saf. Benchmark Eval. Project Handb. NEA/NSC/DOC(95)03/I, NEA 7329, OECD Nuclear Energy Agency, Paris.

Harvey, J., Private communication, X4: 13732001.

Herman, M., Trkov, A., 2010. ENDF-6 Formats Manual. National Nuclear Data Center, Brookhaven National Laboratory Upton, NY.

Horen, D.J., Harvey, J.A., Hill, N.W., 1978. Doorway states in s-, p-, and d-wave entrance channels in ^{207}Pb+n reaction. Phys. Rev. C 18, 722–735. http://dx.doi.org/10.1103/PhysRevC.18.722, URL https://link.aps.org/doi/10.1103/PhysRevC.18.722.

Horen, D.J., Harvey, J.A., Hill, N.W., 1979. ^{206}Pb+n Resonances for E = 25 − 600 kev: s-, p-, and d-wave doorway states and M1 ground-state radiative strength in ^{207}Pb. Phys. Rev. C 20, 478–496. http://dx.doi.org/10.1103/PhysRevC.20.478, URL https://link.aps.org/doi/10.1103/PhysRevC.20.478.

Iwamoto, O., Iwamoto, N., Shibata, K., Ichihara, A., Kunieda, S., Minato, F., Nakayama, S., 2020. Status of JENDL. EPJ Web Conf. 09002-1-6, 239.

Kahler, A.C., Muir, D.W., Haeck, W., et al., 2019. The NJOY Nuclear Data Processing System: Version 2016. Los Alamos National Laboratory, Los Alamos, NM, LA-UR-17-20093.

Kawano, T., 2016. Optical and Hauser-Feshbach Statistical Model Code: CoH (ver. 3.5) Manual. Theoretical Division, T-2, Los Alamos National Laboratory.

Larson, N.M., 2008. Updated User's Guide for SAMMY: Multilevel R-Matrix Fits to Neutron Data Using Bayes Equations. Oak Ridge National Laboratory, Oak Ridge, TN, ORNL/TM-9179/R8 ENDF-364/R2.

Larson, D.C., Larson, N.M., Harvey, J.A., 1984. ORELA Flight Path 1: Determinations of Its Effective Length vs Energy, Experimental Energies, and Energy Resolution Function and Their Uncertainties, ORNL/TM-8880. Oak Ridge National Laboratory.

Lee, M., et al., 2020. HIGHLY ENRICHED URANIUM METAL SPHERES AND CYLINDERS reflected BY LEAD: HEU-met-FAST-057. Int. Crit. Saf. Benchmark Eval. Project Handb. NEA/NSC/DOC(95)03/II, NEA 7329, OECD Nuclear Energy Agency, Paris.

Lell, R., et al., 2020. ZPR-3 Assembly 59: A cylindrical assembly of plutonium metal and graphite with a thick lead reflector: PU-MET-Inter-004. Int. Crit. Saf. Benchmark Eval. Project Handb. NEA/NSC/DOC(95)03/I, NEA 7329, OECD Nuclear Energy Agency, Paris.

Lyutov, V.D., et al., 2020. Three cylinders of lead-reflected highly enriched uranium: HEU-met-Fast-064. Int. Crit. Saf. Benchmark Eval. Project Handb. NEA/NSC/DOC(95)03/II, NEA 7329, OECD Nuclear Energy Agency, Paris.

Macklin, R.L., Gibbons, J.H., 1969. ^{208}Pb(n, γ) Cross sections by activation between 10 and 200 kev. Phys. Rev. 181, 1639–1642. http://dx.doi.org/10.1103/PhysRev.181.1639, URL https://link.aps.org/doi/10.1103/PhysRev.181.1639.

Mamtimin, M., et al., 2018. High power liquid lead-bismuth targetry for intense fast neutron sources using a superconducting electron linac. In: 2018 High Power Targetry Workshop.

Manturov, G., et al., 2020. Neutron and photon leakage spectra from CF-252 source at centers of three lead spheres of different diameters: alarm-CF-pb-shield-001. Int. Crit. Saf. Benchmark Eval. Project Handbook NEA/NSC/DOC(95)03/VIII, NEA 7329, OECD Nuclear Energy Agency, Paris.

der Marck, S.C.V., et al., 2012. Benchmarking ENDF/B-VII.1, JENDL-4.0 and JEFF-3.1.1 with MCNP6. Nucl. Data Sheets 113.

Mihailescu, L.C., Borcea, C., Baumann, P., Dessagne, P., Jericha, E., Karam, H., Kerveno, M., Koning, A., Leveque, N., Pavlik, A., Plompen, A., Quétel, C., Rudolf, G., Trešl, I., 2008. A measurement of (n,xnγ) cross sections for ^{208}pb from threshold up to 20 MeV. Nuclear Phys. A 811 (1), 1–27. http://dx.doi.org/10.1016/j.nuclphysa.2008.07.016, URL https://www.sciencedirect.com/science/article/pii/S0375947408006301.

Mihailescu, L., Plompen, A., 2006. Neutron (n,xngamma) Cross-Section Measurements for ^{52}Cr, ^{209}Bi and ^{206,207,208}Pb from Threshold up to 20MeV (Ph.D. thesis). Office for Official Publications of the European Communities, University of Bucharest, Faculty of Physics, Bucharest (Romania), Luxembourg (Luxembourg).

Miller, T., et al., 2020. Neutron activation foil and thermoluminescent dosimeter responses to a lead reflected pulse of the CEA valduc silene critical assembly: alarm-tran-PB-shield-001. Int. Crit. Saf. Benchmark Eval. Project Handb. NEA/NSC/DOC(95)03/VIII, NEA 7329, OECD Nuclear Energy Agency, Paris.

Moldauer, P.A., 1963. Average resonance parameters and the optical model. Phys. Rev. 129, 754–756. http://dx.doi.org/10.1103/PhysRev.129.754, URL https://link.aps.org/doi/10.1103/PhysRev.129.754.

Negret, A., Mihailescu, L.C., Borcea, C., Dessagne, P., Guber, K.H., Kerveno, M., Koning, A.J., Olacel, A., Plompen, A.J.M., Rouki, C., Rudolf, G., 2015. Cross section measurements for neutron inelastic scattering and the (n, 2nγ) reaction on ^{206}Pb. Phys. Rev. C 91, 064618. http://dx.doi.org/10.1103/PhysRevC.91.064618, URL https://link.aps.org/doi/10.1103/PhysRevC.91.064618.

Plompen, A., Cabellos, O., Jean, C.D.S., et al., 2020. The joint evaluated fission and fusion nuclear data library, JEFF-3.3. Eur. Phys. J. 181.

Prohaska, T., Irrgeher, J., Benefield, J., Böhlke, J.K., Chesson, L.A., Coplen, T.B., Ding, T., Dunn, P.J.H., Gröning, M., Holden, N.E., Meijer, H.A.J., Moossen, H., Possolo, A., Takahashi, Y., Vogl, J., Walczyk, T., Wang, J., Wieser, M.E., Yoneda, S., Zhu, X.-K., Meija, J., 2022. Standard atomic weights of the elements 2021 (IUPAC technical report). Pure Appl. Chem. 94 (5), 573–600. http://dx.doi.org/10.1515/pac-2019-0603.

Ratzel, U., Arlandini, C., Käppeler, F., Couture, A., Wiescher, M., Reifarth, R., Gallino, R., Mengoni, A., Travaglio, C., 2004. Nucleosynthesis at the termination point of the s process. Phys. Rev. C 70, 065803. http://dx.doi.org/10.1103/PhysRevC.70.065803, URL https://link.aps.org/doi/10.1103/PhysRevC.70.065803.

Rozhikhin, Y., et al., 2020. BFS-61 assemblies: critical experiments of mixed plutonium, depleted uranium, graphite and lead with different reflectors: mix-met-Fast-006. Int. Crit. Saf. Benchmark Eval. Project Handb. NEA/NSC/DOC(95)03/VI, NEA 7329, OECD Nuclear Energy Agency, Paris.

Saglime, F.J., Danon, Y., Block, R.C., Rapp, M.J., Bahran, R.M., Leinweber, G., Barry, D.P., Drindak, N.J., 2010. A system for differential neutron scattering experiments in the energy range from 0.5 to 20 MeV. Nucl. Instrum. Methods Phys. Res., Sect. A 620, 401–409. http://dx.doi.org/10.1016/j.nima.2010.04.051.

dos Santos, A., do Nascimento, J.A., 2002. An integral lead reactor concept for developing countries. Nucl. Technol. 140, 233–254.

Sears, V.F., 1962. Bound Coherent and Incoherent Thermal Neutron Scattering Cross Sections of the Elements. Chalk River Nuclear Laboratories, Atomic Energy of Canada Limited, AECL-7980.

Smith, G., 2010. Lead-Cooled Fast Reactor (LFR) Design: Safety, Neutronics, Thermal Hydraulics, Structural Mechanics, Fuel, Core, and Plant Design. Lawrence Livermore National Laboratory, LLNL-BOOK-424323.

Smith, D.L., 2011. Quality Assurance Requirements for ENDF/B-VII.1 Covariances. CSWEG Committee, ENDF-377.

Weissman, L., Tessler, M., Arenshtam, A., Eliyahu, I., Halfon, S., Guerrero, C., Kaizer, B., Kijel, D., Kreisel, A., Palchan, T., Paul, M., Perry, A., Schimel, G., Silverman, I., Shor, A., Tamim, N., Vaintraub, S., 2017. Measurement of ^{208}Pb(n, γ)^{209}Pb maxwellian averaged neutron capture cross section. Phys. Rev. C 96, 015802. http://dx.doi.org/10.1103/PhysRevC.96.015802, URL https://link.aps.org/doi/10.1103/PhysRevC.96.015802.

Werner, C.J., 2017. MCNP Users Manual - Code Version 6.2. Los Alamos National Laboratory, Los Alamos, NM, LA-UR-17-29981.

Youmans, A., Brown, J., Daskalakis, A., Thompson, N., Weltz, A., Danon, Y., McDermott, B., Leinweber, G., Rapp, M., 2015. Fast neutron scattering measurements with lead. Accelerator Appl. 15.

Zrondnikov, A.V., Chitaykin, V.I., et al., 2000. Use of Russian Technology of Ship Reactors with Lead-Bismuth Coolant in Nuclear Power. Tech. rep., Institute of Physics and Power Engineering, Obninsk, Russia.